Characterization and FTIR Studies of MnO_x-CeO_2 Catalyst for Low-Temperature Selective Catalytic Reduction of NO with NH_3

Gongshin Qi and Ralph T. Yang*

Department of Chemical Engineering, University of Michigan, Ann Arbor, Michigan 48109-2136

Received: April 8, 2004; In Final Form: July 23, 2004

A series of high-activity manganese−cerium oxide catalysts for the low-temperature (373−453 K) selective catalytic reduction (SCR) of NO_x with ammonia were prepared. They were prepared by using the citric acid method (CA), coprecipitation method (CP), and impregnation method (IM) and were characterized by XRD, ESR, XPS, and FTIR techniques. A sample prepared by the CA method, $MnO_x(0.3)-CeO_2(923)$, showed the highest activity. XRD results showed that the catalyst prepared by the CA method had the smallest particle size and the weakest XRD peak intensity. Using ESR and XPS, Mn^{4+}, Mn^{3+}, and Mn^{2+} oxide species were found after calcination in air. Three kinds of Mn phases existed in the MnO_x-CeO_2 catalysts that were prepared by the CA method: (1) aggregated Mn_2O_3 on the CeO_2 support, (2) highly dispersed Mn_2O_3 with strong interactions with CeO_2, and (3) Mn atoms incorporated into the CeO_2 lattice. The distribution of Mn species depends on the preparation methods. Any oxygen vacancy formed in the CeO_2 lattice caused by incorporation of Mn atoms adsorbs and activates molecular oxygen to form active oxygen species. Thus, the high activity of $MnO_x(0.3)-CeO_2(923)$ is attributed to the highly dispersed Mn species and the more active oxygen species that is formed. Ammonia molecules adsorbed onto $MnO_x(0.3)-CeO_2(923)$ to form NH_4^+ and coordinated NH_3. At the same time, NH_2 was observed because of H-abstraction. NO_2, nitrite, and nitrate were formed by oxidation of NO. A mechanistic pathway for this reaction was proposed on the basis of earlier findings and the FTIR results obtained in this work. The initial step was adsorption of NH_3 onto the Lewis acid sites, and then, the NH_2 species was formed, followed by reaction between NH_2 and NO to produce N_2 and H_2O. Possible intermediates are proposed, and all the intermediates could transform into NH_2NO, which could further react to produce N_2 and H_2O.

1. Introduction

Nitrogen oxides (NO, NO_2, and N_2O) resulting from combustion remain a major source for air pollution. They contribute to photochemical smog, acid rain, ozone depletion, and greenhouse effects. Nearly all (95%) of the NO_x derives from transportation (49%) and power plants (46%). The current technology for reducing nitrogen oxide emissions from power plants is selective catalytic reduction (SCR) of NO_x ($x = 1, 2$) with ammonia as the reducing agent. Many catalysts have been reported to be active for this reaction. They are mainly divided into two groups: mixed oxides and ion-exchange molecular sieves.[1,2] In the automotive catalytic converters, the reducing agent could be CO[3,4] and hydrocarbons,[5−9]

The commercial catalyst for this process is V_2O_5/TiO_2 (anatase) catalyst promoted by WO_3 or MoO_3.[10−19] The addition of WO_3 and/or MoO_3 to V_2O_5/TiO_2 can increase the activity for ammonia SCR, reduce ammonia oxidation, and greatly increase the poison resistance of the catalysts to alkali and arsenious oxides. Although the SCR technology based on vanadia catalysts has been commercialized, problems still remain. These problems include high activity for oxidation of SO_2 to SO_3, formation of N_2O at high temperatures, and toxicity of vanadia. The oxidation of SO_2 to SO_3 is a problem because SO_3 combines with NH_3 and H_2O, resulting in the formation of NH_4HSO_4, $(NH_4)_2S_2O_7$, and H_2SO_4, which cause corrosion and plugging of equipment. Although N_2O is known as the most stable greenhouse gas, its creation is a problem because it is involved in the destruction of the ozone layer. Because of these drawbacks for vanadia catalysts, many are working to develop new catalysts for the ammonia SCR reaction.

For the reasons listed, there has been strong interest in developing highly active catalysts for low-temperature SCR. Such a catalyst would be placed downstream of the desulfurizer and electrostatic precipitator, operating at a temperature of 423−433 K. Success in developing such a catalyst would significantly improve the economics of SCR. However, some problems arise from these operating conditions. First, there is still residual SO_2 remaining after the desulfurizer. Thus, SO_2 resistance needs to be considered. The main disadvantage of low-temperature SCR is its susceptibility to ammonium bisulfate precipitation and formation of solid ammonium salts with NO_2 (especially ammonium nitrate). This effect could be minimized by increasing the catalyst volume to provide spare surface area for deposition and by periodically operating at higher temperatures to evaporate the deposited ammonium bisulfate.

Some transition-metal-containing catalysts have been investigated for the low-temperature SCR reaction, such as chromia,[2] $NiSO_4/Al_2O_3$,[20] MnO_x/Al_2O_3,[21] V_2O_5/activated carbon,[22] iron−silica aerogels,[23] MnO_x/NaY,[24] MnO_x/TiO_2,[69,70] and other oxides.[25] They have shown various SCR activities below 473 K under different conditions. Recently, we found that Fe−Mn-based transition-metal oxides[26] were highly active for low-temperature SCR of NO with NH_3 with 100% selectivity to N_2 at a high space velocity.

* Corresponding author. Phone: (734)-936-0771. Fax: (734)-763-0459. E-mail address: yang@umich.edu.

10.1021/jp048431h CCC: $27.50
Published on Web 09/08/2004

Ceria (CeO_2) has been studied extensively for its oxygen storage and redox properties. For example, ceria has been used as an important component of three-way catalysts (TWCs).[27−29] The most important property of ceria is as an oxygen reservoir, which stores and releases oxygen via the redox shift between Ce^{4+} and Ce^{3+} under oxidizing and reducing conditions, respectively. Ceria should enhance the oxidization of NO to NO_2, thereby increasing the activity of SCR of NO by ammonia.

Our previous studies[30,31] show that MnO_x-CeO_2 is a superior catalyst for NO reduction by NH_3 in the low-temperature window of 373−453 K. The catalyst yielded high N_2 selectivity and nearly complete NO conversion at temperatures as low as 423 K and gas hourly space velocity (GHSV) = 42 000 h^{-1}.[30] Recently, EPRI investigated the intrinsic activity of 100 g batches of $MnO_x(0.3)-CeO_2(923)$ prepared by the CP method and demonstrated excellent activity.[36] At 423 K, the $MnO_x(0.3)-CeO_2(923)$ catalyst had about 50% of the intrinsic activity of conventional $V_2O_5-TiO_2$ SCR catalysts at 623 K. At 473 K, the $MnO_x(0.3)-CeO_2(923)$ catalyst was approximately 90% as active. These results are encouraging in that high intrinsic catalyst activities were achievable at much lower temperatures than conventional SCR.[36] Though we have studied the activity of manganese−cerium oxides for low-temperature SCR of NO with ammonia, characterization of this system and the catalytic mechanism have not been studied.

Unlike high-temperature SCR of NO with ammonia, there have been few studies on the kinetics or mechanism of low-temperature SCR. Kijlstra et al.[66] studied low-temperature SCR over 2 wt % Mn/Al_2O_3 catalyst at 423 K and were able to derive rate equations and Langmuir−Hinshelwood (LH) and Eley−Rideal (ER) pathways to N_2 production. Marbán and Fuertes[67] studied low-temperature SCR over iron-oxides-supported activated carbon fiber and found that the strength of adsorption of NO during the low-temperature SCR reaction would determine the reaction mechanism. A highly stable nitrate is formed on the surface, causing catalyst deactivation and slow reaction through an ER mechanism; NO reacts from the gas phase. The absence of this nitrate permits reaction of less-stable nitrites on the catalyst surface, following an LH-type mechanism. Richter et al.[24] studied low-temperature SCR on MnO_x/NaY composite catalysts and reported the presence of a symmetric O═N−O−N═O species (formally corresponding to N_2O_3) on the composite catalyst after contact with NO. The catalyst performance was associated with a close coupling of nitrite formation and its drain-off from equilibrium with NO/NO_2 and nitrate by ammonia. Kapteijn et al.[58] proposed a model where ammonia was successively dehydrogenated by surface oxygen, forming nitric oxide in the limit. The intermediate surface species ($-NH_2$) could react with nitric oxide to form nitrogen. In this work, we characterized the manganese−cerium oxides catalyst and investigated the catalytic mechanism of the low-temperature SCR by FTIR.

2. Experimental Section

Catalyst Preparation. *1. Citric Acid Method (CA).* Manganese nitrate ($Mn(NO_3)_2{\cdot}4H_2O$, 98%, from Sigma), cerium nitrate ($Ce(NO_3)_3{\cdot}6H_2O$, 99%, from Aldrich), and citric acid (anhydrous, $C_6H_8O_7$, from Sigma) were mixed in desired proportions. The mole ratio of citric acid to the metal components (the total moles of manganese and cerium) was 1.0. The mixture was stirred at room temperature for 1 h. The solution was dried at 373 K, resulting in a porous, foamlike solid. The foamlike precursor was calcined in air at a desired temperature for 6 h. The obtained solid sample was first dried at 393 K in air for 12 h and then calcined at 923 K for 6 h in air in a tubular furnace. Finally, the samples were crushed and sieved to 60−100 mesh. Pure manganese oxide and ceria catalysts were prepared by the same procedure. The catalyst is denoted as $MnO_x(z)-CeO_2(y)$. *z* represents the mole ratio of Mn/(Mn + Ce), and *y* denotes the calcination temperature in K (e.g., $MnO_x(0.3)-CeO_2(923)$).

2. Impregnation Method (IM). In this method, we used incipient wetness impregnation. The desired amount of manganese acetate solution was added to a certain amount of cerium oxide. The obtained solid sample was first dried at 393 K in air for 12 h and then calcined at 923 K for 6 h in a tubular furnace. Finally, the samples were crushed and sieved to 60−100 mesh.

3. Coprecipitation Method (CP). In this work, a certain amount of salts (mentioned already) of Mn and Ce were dissolved in water, excess urea was added to the solution, and then the temperature was increased slowly to 363 K with stirring. The mixtures were aged for several hours and then filtered and washed with deionized water. The obtained solid samples were first dried at 393 K in air for 12 h and then calcined at 923 K for 6 h in a tubular furnace. Finally, the samples were crushed and sieved to 60−100 mesh.

Catalyst Characterization. The powder X-ray diffraction (XRD) measurements were carried out with a Rigaku Rotaflex D/Max-C system with Cu Kα (λ = 0.1543 nm) radiation. The samples were loaded on a sample holder with a depth of 1 mm. The mean crystallite size of the cubic phase was calculated from the Scherrer equation, where the Scherrer constant (particle shape factor) was taken as 0.89. The lattice parameters were calculated by the square method according to the Cohen procedure.[32]

The XPS experiment was carried out on a Perkin-Elmer PHI 5400 ESCA system at room temperature under $10^{-8}-10^{-9}$ Torr, using Mg Kα radiation. Manganese and cerium oxides binding energies were calibrated relative to the carbon impurity with a *C1s* at 284.5 eV.

ESR spectra were recorded on a Brucker EMX ESR spectrometer, under the conditions of a microwave of 0.202 mW and a modulation amplitude of 1.0 G. Before recording the spectra, the samples were flushed with He to remove weakly adsorbed oxygen and other impurities.

Catalytic Activity Measurement. The SCR activity measurement was carried out in a fixed-bed quartz reactor. The typical reactant gas composition was as follows: 1000 ppm NO, 1000 ppm NH_3, 2% O_2, and balance He. In typical conditions, a 200-mg sample was used in each run. The total flow rate was 100 mL/min (under ambient conditions). Thus, a very high GHSV was obtained (4.2×10^4 L/h). The premixed gases (1.01% NO in He, 1.00% NH_3 in He, and 0.99% SO_2 in He) were supplied by Matheson. Water vapor was generated by passing He through a heated gas-wash bottle containing deionized water. The tubing of the reactor system was heat-traced to prevent formation and deposition of ammonium sulfate/bisulfate and ammonium nitrate. The NO and NO_2 concentrations were continually monitored by a chemiluminescent NO/NO_x analyzer (Thermo Environmental Instruments Inc. model 42C). To avoid errors caused by the oxidation of ammonia in the converter of the NO/NO_x analyzer, an ammonia trap containing phosphoric acid solution was installed before the sample inlet to the chemiluminescent analyzer. The products were also analyzed by a gas chromatograph (Shimadzu, 8 Å) at 323 K with a 5-Å molecular sieve column for N_2 and Porapak Q column for N_2O. Because the reaction was carried out at low temperature (<473 K), it must be confirmed that the decrease of NO was not caused by the adsorption of NO on the catalysts. In each experiment,

we first purged the catalyst with the reaction gas at room temperature until the NO concentration in the outlet reached the inlet gas concentration (1000 ppm). On the basis of such data, we could calculate the nitrogen balance (inlet [NO] = outlet [NO] + [N_2] + [N_2O]). In all of the experiments in this work, the nitrogen balance was more than 95%.

The experiments for reactions between NH_3 and NO_x were carried out under stoichiometric ratios of NO_x/NH_3 according to the following reactions:

$$6NO + 4NH_3 \rightarrow 5N_2 + 6H_2O \quad (1)$$

$$4NO + 4NH_3 + O_2 \rightarrow 4N_2 + 6H_2O \quad (2)$$

$$6NO_2 + 8NH_3 \rightarrow 7N_2 + 12H_2O \quad (3)$$

$$2NH_3 + NO + NO_2 \rightarrow 2N_2 + 3H_2O \quad (4)$$

Thus, the following compositions were used: 1500 ppm NO and 1000 ppm NH_3 for reaction 1, 1000 ppm NO + 1000 ppm NH_3 and 2% O_2 for reaction 2, 750 ppm NO_2 and 1000 ppm NH_3 for reaction 3, and 500 ppm NO, 500 ppm NO_2, and 1000 ppm NH_3 for reaction 4. The total flow rate was 500 mL/min (ambient conditions).

FTIR Study. Infrared spectra were recorded on a Nicolet Impact 400 FTIR spectrometer with a TGS detector. Self-supporting wafers of 1.3-cm diameter were prepared by pressing 15 mg of sample, and then they were loaded into an IR cell with BaF_2 windows. The wafers could be pretreated in situ in the IR cell. The wafers were first treated at 573 K in a flow of high purity O_2/He for 0.5 h and then cooled to room temperature. At each temperature, the background spectrum was recorded in flowing He and was subtracted from the sample spectrum that was obtained at the same temperature. Thus, the IR absorption features that originated from the structure vibrations of the catalyst were eliminated from the sample spectra. In the experiment, the IR spectra were recorded by accumulating 100 scans at a spectra resolution of 4 cm^{-1}.

3. Results

Characterization of Catalysts. The XRD patterns of the Mn−Ce mixed oxides catalysts with various ratios of Mn/(Mn + Ce), calcined at 923 K and prepared by the CA method, are shown in Figure 1. The XRD patterns of these mixed oxides showed broad reflections due to CeO_2 of a cubic fluorite structure. The same phenomena were observed on MnO_x−CeO_2 prepared by the coprecipitation method.[35] This result was consistent with the report of Machida et al.[34] They found diffraction profiles at Mn/(Mn + Ce) > 0.75 showing crystallization of Mn_2O_3, whereas those at Mn/(Mn + Ce) < 0.5 consisted of only broad peaks attributed to CeO_2. The replacement of Ce^{4+} by Mn^{3+} in the fluorite structure was possible because of their structural similarity.[34] Machida et al.[34] proposed that a solid solution was formed between Mn_2O_3 and CeO_2. For the XRD patterns of pure MnO_x and CeO_2, there were intense and sharp peaks. For pure MnO_x calcined at 923 K, crystalline phases of Mn_2O_3 were observed. The crystal structure of Mn_2O_3 is the C-rare earth type that is basically composed of anion-deficient units of fluorite structure.[48] Figure 2 shows the XRD profiles of Mn(0.3)−CeO_2 calcined at different temperatures. All of the catalysts consisted of peaks attributed to CeO_2 with a cubic fluorite (CaF_2) structure,[71] with intensities increasing with the calcination temperature. From Figures 1 and 2, it can be seen that the coexistence of manganese and cerium oxides enhances the dispersion and lowers the crystallinity of both, which indicates that there are strong interactions between these two metal oxides.

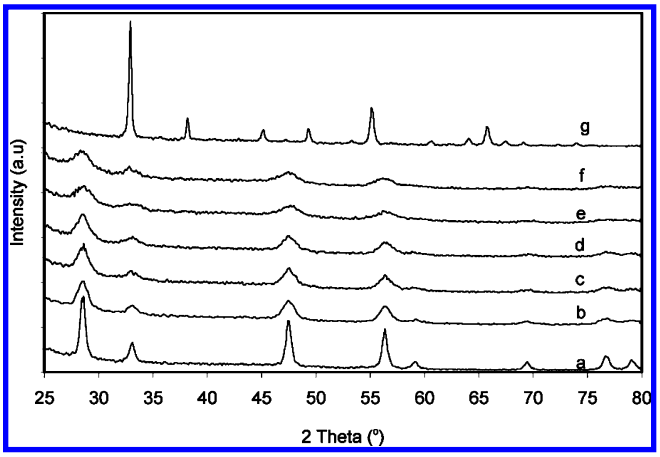

Figure 1. XRD profiles of MnO_x−CeO_2 mixed oxide catalysts with different Mn contents prepared by the CA method. The number in the first parentheses indicates mole fraction of Mn, and that in the second parentheses is calcination temperature in K. (a) CeO_2(923); (b) MnO_x-(0.1)−CeO_2(923); (c) MnO_x(0.2)−CeO_2(923); (d) MnO_x(0.3)−CeO_2-(923); (e) MnO_x(0.4)−CeO_2(923); (f) MnO_x(0.5)−CeO_2(923); (g) MnO_x(923).

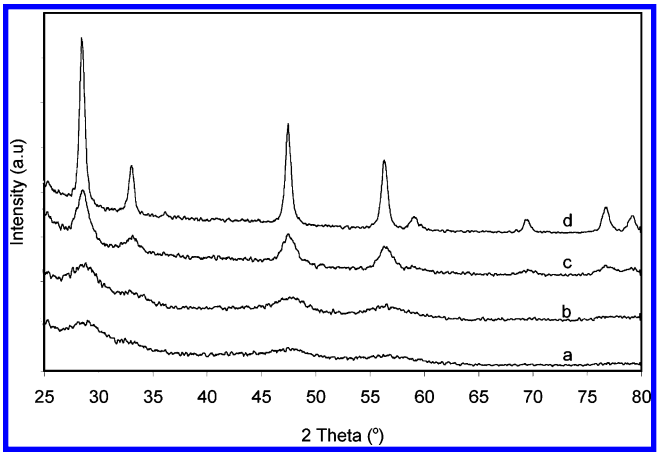

Figure 2. XRD profiles of MnO_x(0.3)−CeO_2 catalysts prepared by the CA method calcined at different temperatures: (a) 673; (b) 773; (c) 923; (d) 1023 K.

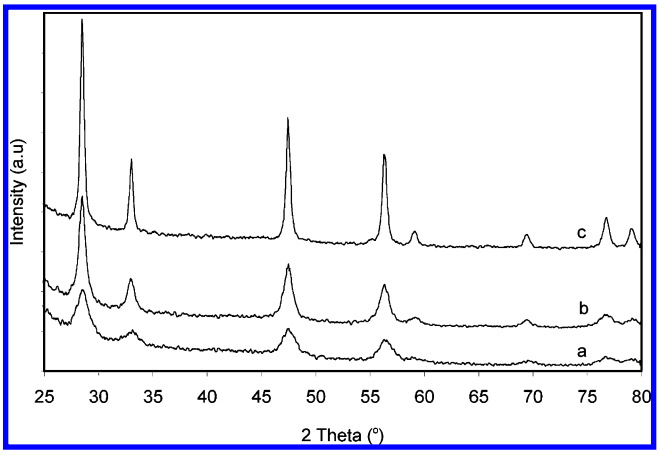

Figure 3. XRD profiles of MnO_x(0.3)−CeO_2(923) prepared by different methods: (a) citric acid method; (b) coprecipitation method; (c) impregnation method.

The XRD profiles of MnO_x(0.3)−CeO_2(923) prepared by different methods are shown in Figure 3. The XRD profiles consisted of peaks attributed to CeO_2 with a cubic fluorite

TABLE 1: Lattice Parameters and Mean Crystallite Size of the Ceria Cubic Phase (111) of MnO_x-CeO_2

catalyst[a]	mean crystallite size (Å)	lattice parameter (Å)
CeO_2	149	5.418
$MnO_x(0.1)-CeO_2(923)$	100	5.413
$MnO_x(0.2)-CeO_2(923)$	95	5.412
$MnO_x(0.3)-CeO_2(923)$	84	5.411
$MnO_x(0.4)-CeO_2(923)$	76	5.411
$MnO_x(0.5)-CeO_2(923)$	70	5.414
$MnO_x(0.3)-CeO_2(923)$ (IM)	178	5.414
$MnO_x(0.3)-CeO_2(923)$ (CP)	127	5.412

[a] Prepared by the CA method unless otherwise marked.

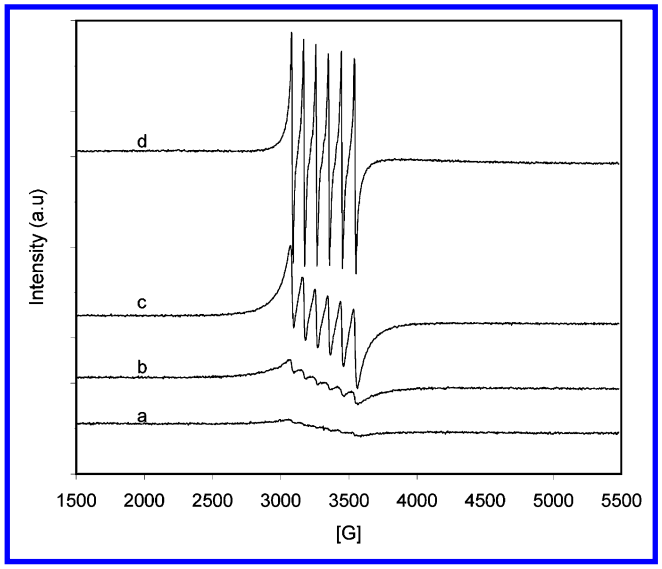

Figure 4. ESR spectra of Mn−Ce mixed oxides calcined at different temperatures: (a) $MnO_x(0.3)-CeO_2(673)$; (b) $MnO_x(0.3)-CeO_2(773)$; (c) $MnO_x(0.3)-CeO_2(923)$; (d) $MnO_x(0.3)-CeO_2(1023)$.

structure, but the peaks of CeO_2 were broader on the $MnO_x(0.3)-CeO_2(923)$ prepared by the CA method than others. From Figure 3, it can be seen that the $MnO_x(0.3)-CeO_2(923)$ prepared by the IM method has the highest XRD intensity, which means that the Mn and Ce oxides have the weakest interactions.

Table 1 lists the lattice parameters and the mean crystallite sizes of the ceria cubic phase in MnO_x-CeO_2 with different contents of manganese oxide. It can be seen that the lattice parameters of ceria decrease with the addition of Mn, suggesting that some Mn^{3+} ions are incorporated into the ceria lattice to form a solid solution, because the radius of Mn^{3+} ions (0.065 nm) is smaller than that of Ce^{4+} ions (0.094 nm). The mean crystallite size of ceria decreases with increasing Mn content, indicating that Mn atoms incorporated into CeO_2 inhibit the crystal growth of ceria. Similar observations were reported by Shan et al.[33] and Machida et al.[34]

On the basis of Figure 3, for these three catalysts, the catalyst prepared by the impregnation method had the strongest CeO_2 crystalline diffraction peaks. The catalyst prepared by the citric acid method had the weakest CeO_2 diffraction peaks. The mean crystalline size (Table 1) of the catalysts prepared by different methods also shows that the catalyst prepared by the citric acid method had the smallest size.

ESR spectroscopy was used to study the oxidation states and the chemical environment of the Mn species present in these samples. Usually, Mn^{3+} is ESR silent owing to its large zero-field splitting; both Mn^{2+} and Mn^{4+} can give similar ESR spectra.[37−40] Figure 4 shows the ESR spectra of $Mn(0.3)-CeO_2$ calcined at various temperatures. All samples show six hyperfine

TABLE 2: ESR Parameters of Mn^{2+} in $Mn(0.3)-CeO_2$ Calcined at Various Temperatures

calcination temp (K)	*g* factor	*A* (G)
673	2.000	92.4
773	2.006	92.2
923	2.007	92.0
1023	2.009	91.4

TABLE 3: XPS of Mn $2p_{3/2}$ in $Mn(0.3)-CeO_2$ Calcined at Various Temperatures

calcination temp (K)	phase	binding energy (eV)	concn (%)
673	Mn^{2+}	640.3	15.2
	Mn^{3+}	641.6	56.0
	Mn^{4+}	643.2	28.8
773	Mn^{2+}	640.5	19.1
	Mn^{3+}	642.0	52.9
	Mn^{4+}	643.3	28.0
923	Mn^{2+}	640.6	24.4
	Mn^{3+}	641.9	49.7
	Mn^{4+}	643.6	25.9
1023	Mn^{2+}	640.7	30.8
	Mn^{3+}	642.3	50.6
	Mn^{4+}	644.5	18.6

lines similar to those observed previously.[37−40] The *g* factors of these ESR patterns were centered at 2.0 with an average hyperfine coupling constant *A* of approximately 90 G (see Table 2), indicating that the Mn in these samples retained its +2 oxidation state, because Mn^{4+} would show a *g* value of <2 and an *A* value of approximately 76 G. However, differences are observed in the ESR pattern intensities of the $Mn(0.3)-CeO_2$ calcined at various temperatures. A significant increase in intensity was observed when the calcination temperature was increased. The increase of calcination temperature resulted in an increase of the ESR intensity, possibly because of an increase in the content of Mn^{2+}. Most of the ESR studies on Mn^{2+}-containing materials reported an octahedral or axially distorted octahedral coordination of Mn^{2+} ions.[37−40] ESR results shown in Table 2 suggest that the coordination of the Mn^{2+} ions could be assigned as axially distorted octahedral. From Table 2, both *g* and *A* values can be assigned to Mn^{2+}. However, it cannot exclude the existence of Mn^{4+} ions entirely, because the observed Mn^{2+} signal could possibly superimpose on the Mn^{4+} signal.[38]

To further study the oxidation states of manganese in the Mn−Ce mixed oxide, XPS spectra were taken on the $MnO_x(0.3)-CeO_2$ calcined at different temperatures. The XPS measurements of the Mn $2p_{3/2}$ in $Mn(0.3)-CeO_2$ calcined at various temperatures are shown in Table 3, and the surface concentrations of different manganese states were also shown in Table 3. From Table 3, it can be seen that Mn^{4+}, Mn^{3+}, and Mn^{2+} oxide species were found after calcination at 673−1023 K in air. Binding energies between 640 and 645 eV were found which were higher than the binding energies for MnO, MnO_2, and Mn_2O_3.[62,63] This may indicate a strong interaction between manganese and cerium oxides, similar to that found for surface manganese oxide on alumina[65] and manganese oxide−silica aerogels.[64]

FTIR Spectra of Nitrogen Oxide Adsorption on Mn−Ce Mixed Oxide Catalyst. Many groups have studied NO_x adsorption on ion-exchange zeolites and metal oxides, and IR bands due to adsorbed NO_2, nitrite, and nitrate (NO_3^-) species were detected in the 1650−1000 cm^{-1} range.[41−45,71] $MnO_x(0.3)-CeO_2(923)$ prepared by the CA method was first heated at 573 K for 0.5 h in a flow of O_2/He and then cooled to room temperature in He for adsorption of NO/He, NO + O_2/He, and NO_2/He. Figure 5 shows the IR spectra after these gases were

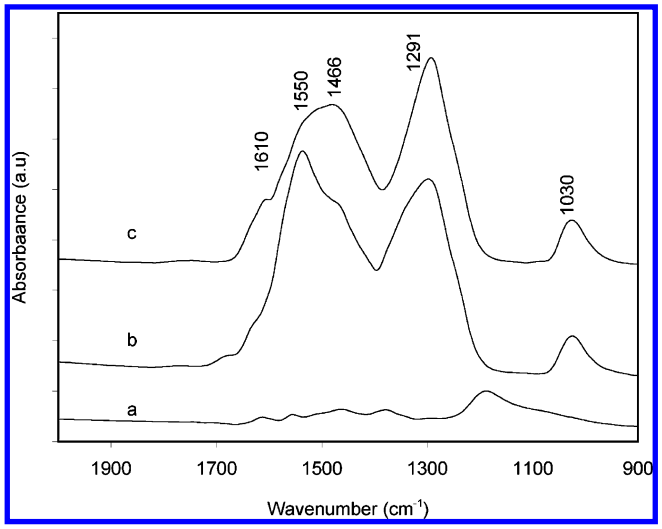

Figure 5. IR spectra of $MnO_x(0.3)-CeO_2(923)$ treated with (a) 1000 ppm NO, (b) 1000 ppm NO_2, and (c) 1000 ppm NO + 2% O_2 at room temperature for 30 min and then purged by He for 30 min.

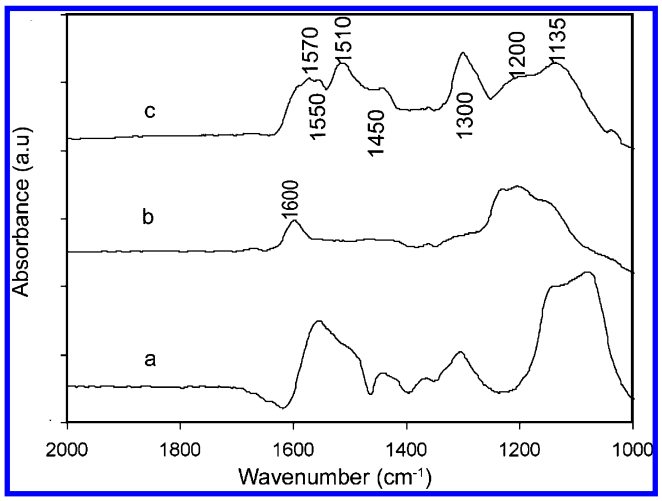

Figure 6. IR spectra of $MnO_x(0.3)-CeO_2(923)$ treated in flowing 1000 ppm NO + 2% O_2 at room temperature for 30 min and then purged by He at (a) 298, (b) 353, (c) 393, (d) 423, and (e) 453 K.

adsorbed for 30 min followed by purging in He for another 30 min. In the spectrum of NO adsorbed on $MnO_x(0.3)-CeO_2(923)$ catalyst, some very weak bands were observed (Figure 5a). After the catalyst was treated in flowing NO + O_2/He for 30 min, five bands at 1610, 1550, 1466, 1291, and 1030 cm^{-1} were formed (Figure 5c). These bands were also observed in the spectrum of NO_2 adsorbed on this catalyst (Figure 5b), but their intensities were stronger than those of the NO + O_2/He treated sample. Similar IR bands were also detected in the spectrum of NO_2 adsorbed on TiO_2 by Ramis et al.[41] The bands at 1550, 1291, and 1030 cm^{-1} can be assigned to bidentate nitrate;[71] the band at 1466 cm^{-1} can be attributed to the monodentate nitrite.[71]

Figure 6 shows a series of IR spectra of NO + O_2 adsorbed on $MnO_x(0.3)-CeO_2(923)$ followed by purging at different temperatures in helium. After $MnO_x(0.3)-CeO_2(923)$ was treated in flowing NO + O_2/He for 1 h at room temperature and then purged by He for 30 min, strong bands were observed at 1400−1650, 1291, and 1030 cm^{-1}, which are the same as in Figure 5c. With an increase in temperature to 353 K in a flow of He, the bands at 1466 and 1291 cm^{-1} shifted to new bands at 1580, 1540, and 1230 cm^{-1}. With an increase in temperature to 423 K, the band at 1610 cm^{-1} almost vanished, while the intensities of other bands decreased with an increase in temperature.

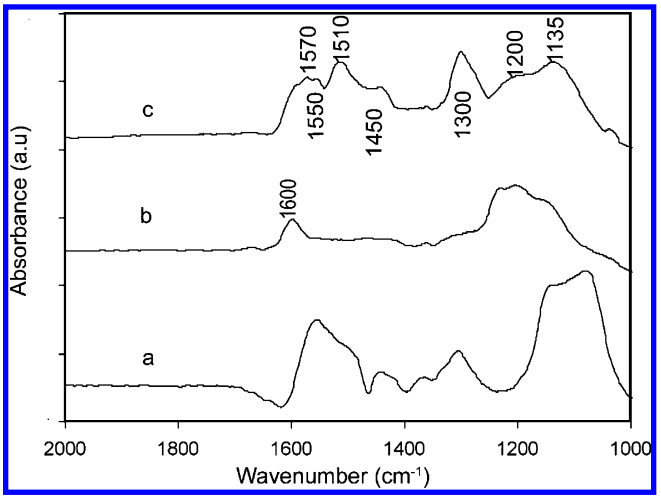

Figure 7. FTIR spectra of chemisorbed NH_3 at 298 K on various catalysts prepared by the CA method: (a) $CeO_2(923)$; (b) $MnO_x(923)$; (c) $MnO_x(0.3)-CeO_2(923)$.

The bands at 1580, 1540, and 1291 cm^{-1} were attributed to nitrate species as mentioned already. The band at 1610 cm^{-1} is very close to the asymmetric stretching frequency of gaseous NO_2 molecules (1617 cm^{-1}).[42] We assign it to an NO_2 adspecies on the catalyst because this species had a thermal stability different from those of other adsorbed nitrate species (Figure 6). The band at 1230 cm^{-1} is very close to the bridging nitrite species reported in the literature,[71] so it was assigned to the bridged nitrite. The results indicated that NO could be oxidized readily to NO_2, nitrite, and nitrate species on this catalyst in the presence of oxygen.

IR Spectra of NH_3 Adsorption on Mn−Ce Mixed Oxide Catalyst. $MnO_x(0.3)-CeO_2(923)$ prepared by the CA method was first heated at 573 K for 0.5 h in a flow of O_2/He and then cooled to room temperature in He for adsorption of NH_3/He. FTIR spectra (Figure 7a) of NH_3 adsorbed on CeO_2 showed strong bands at 1570, 1300, and 1200−1000 cm^{-1} and two weak bands at 1450 and 1510 cm^{-1}. On MnO_x (Figure 7b), one strong band at 1600 cm^{-1} and a wide band around 1000−1300 cm^{-1} were observed. For MnO_x-CeO_2 (Figure 7c), several bands at 1600, 1570, 1550, 1510, 1450, 1300, 1200, and 1135 cm^{-1} were detected. It is known that ammonia that adsorbs on acid catalysts yields two strong bands near 1600 and 1200 cm^{-1}. The band at the higher frequency is typical of the asymmetric deformation of coordinated ammonia; the lower-frequency band is typical of the corresponding symmetric deformation mode. Recently, Busca and co-workers[72−74] have investigated the adsorption of ammonia (NH_3), hydrazine (N_2H_4), and hydroxylamine (NH_2-OH) on various transition-metal-oxide-supported catalysts. The bands below 1600 cm^{-1} are usually not adsorbed NH_3, but they can be assigned to species arising from the reaction of ammonia, adsorbed over acid sites, with redox surface sites of the catalyst (on the basis of the report of Busca et al.).[72−74] The bands centered at 1600 and 1200 cm^{-1} are attributed to the asymmetric and symmetric deformation of coordinated ammonia, respectively. The band at 1510 cm^{-1} is attributed to an amide ($-NH_2$) species.[12] The bands at 1550 and 1570 cm^{-1} may be related to the intermediate of oxidation of ammonia.[72−74] The band at 1300 cm^{-1} can be assigned to the symmetric deformation of ammonia coordinatively bonded to one type of the Lewis acid sites.[75] Another very weak band at 1450 cm^{-1} is due to the asymmetric deformation of ammonium ions adsorbed on the Brönsted sites.[75] These results also clearly indicate that the number of Lewis

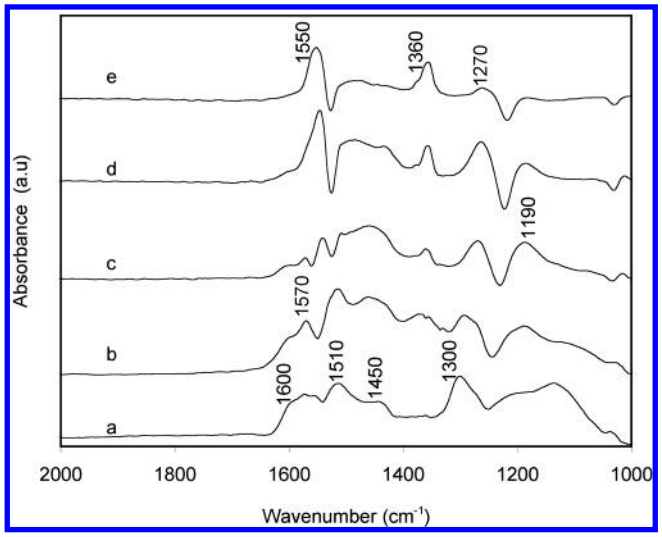

Figure 8. IR spectra of $MnO_x(0.3)-CeO_2(923)$ prepared by the CA method treated in flowing 1000 ppm NH_3 at room temperature for 30 min and then purged by He at (a) 298, (b) 353, (c) 393, (d) 423, and (e) 453 K.

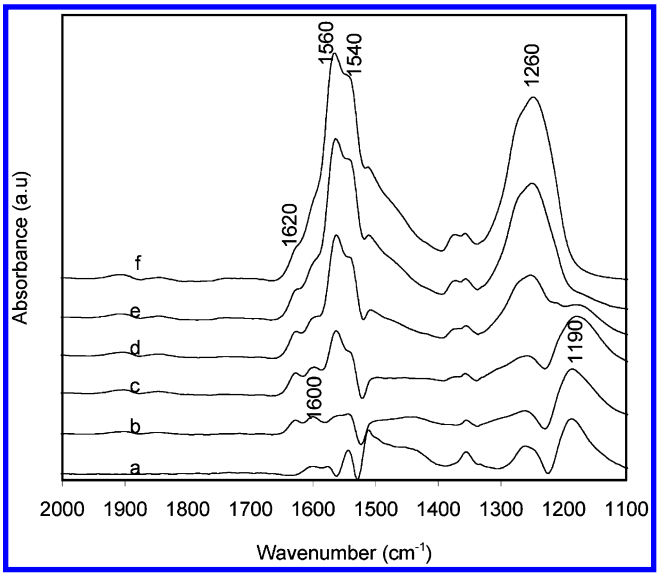

Figure 9. IR spectra taken at 393 K upon passing 1000 ppm NO + 2% O_2 over the NH_3 presorbed on $MnO_x(0.3)-CeO_2(923)$ prepared by the CA method for (a) 0, (b) 0.5, (c) 1.5, (d) 3, (e) 5, and (f) 8 min.

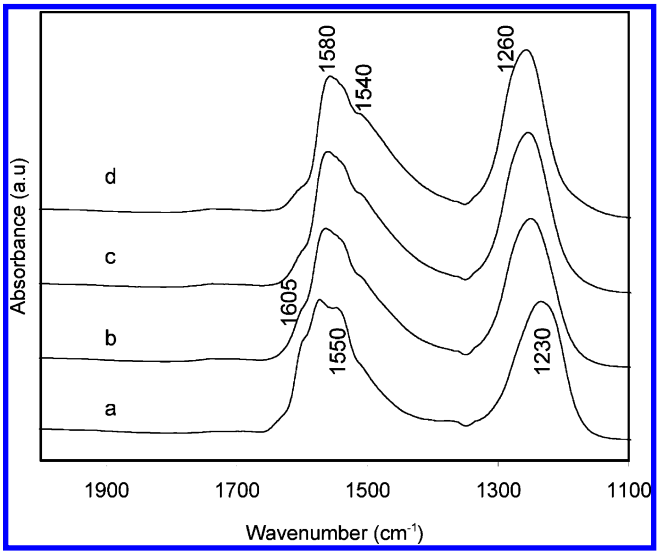

Figure 10. IR spectra taken at 393 K upon passing 1000 ppm NH_3 over the NO + 2% O_2 presorbed on $MnO_x(0.3)-CeO_2(923)$ prepared by the CA method for (a) 0, (b) 0.5, (c) 1.5, and (d) 3 min.

acid sites is much higher than that of Brönsted acid sites on these catalysts.

The FTIR spectra of adsorbed ammonia on $MnO_x(0.3)-CeO_2(923)$ prepared by the CA method at different temperatures are shown in Figure 8. Upon an increase in temperature, the intensities of bands at 1600, 1510, and 1200 cm^{-1} decreased. The bands at 1550 and 1300 cm^{-1} increased first, passing through a maximum at 423 K, and then decreased at higher temperatures. A band at 1360 cm^{-1} was detected, which increased with increasing temperature. The bands at 1550 and 1360 cm^{-1} probably did not belong to any adsorbed ammonia species but could be due to oxidized species such as nitrate or nitrite, as reported by Ramis et al.[72-74] This is not surprising because MnO_x-CeO_2 is highly active for oxidation of ammonia at low temperatures.

IR Spectra of Reacted Species Between Nitrogen Oxides and Ammonia. $MnO_x(0.3)-CeO_2(923)$ was first treated with NH_3/He for 1 h followed by He purged at 393 K. NO + O_2/He was then introduced into the IR cell, and spectra were recorded as a function of time (Figure 9). As noted already, coordinated NH_3 species were formed on $MnO_x(0.3)-CeO_2(923)$ upon treatment with NH_3/He. After NO + O_2/He was passed over the sample for 0.5−8 min, the bands attributed to ammonia adspecies decreased. At the same time, several new weak bands were observed at 1560, 1540, 1260, and 1620 cm^{-1}. The band at 1620 cm^{-1} might come from adsorbed H_2O (a reaction product) or NO_2 or both. The bands at 1560 and 1540 cm^{-1} were attributed to the nitrate species,[46] and the band at 1260 cm^{-1} may be attributed to the nitrite species. These results showed that a reaction between ammonia adspecies (mainly coordinated NH_3) and NO occurred. After 5 min, all of the ammonia adspecies bands diminished (on the basis of the diminished band at 1190 cm^{-1}). The band intensity at 1620 cm^{-1} increased during the first 5 min and then decreased. Hence, we can reasonably attribute this band to H_2O, not NO_2. From Figure 9, it can also be seen that the band at 1510 cm^{-1} diminished very quickly; after 1.5 min, the band at 1510 cm^{-1} disappeared. After 3 min, a band at 1510 cm^{-1} could be detected, which can be assigned to the NO_x species, not amide species ($-NH_2$). On the basis of Figure 9, it can be concluded that NO readily reacts with the adsorbed ammonia species at a very low temperature (at 393 K). The reaction rate between amide species and NO_x is faster than the reaction between NO and the coordinated ammonia (at 1190 cm^{-1}).

IR Spectra of the Reacted Species Between NH_3 and NO_x. In this experiment, the reactants were introduced to the $MnO_x(0.3)-CeO_2(923)$ catalyst in the reversed order. The sample was first treated with NO + O_2/He at 393 K for 1 h and then purged with He for 30 min. NO_2 (1605 cm^{-1}), nitrate species (1580, 1550 cm^{-1}), and nitrite species (1230 cm^{-1}) were formed (Figure 10). NH_3/He was then passed over the NO_x-adsorbed catalyst, and the IR spectra were recorded as a function of time, shown in Figure 10. After NH_3/He was introduced into the cell, the bands due to NO_2 species at 1605 cm^{-1} decreased, and the peak at 1230 cm^{-1} shifted to 1260 cm^{-1}. The spectra obtained from the reaction between ammonia and adsorbed NO_x species at different times are relatively similar; two wide bands at 1580 and 1260 cm^{-1} were observed which may be attributed to nitrate species formed by oxidation of ammonia. This result indicates that the reaction between ammonia and nitrate is unlikely to have occurred, except for the reaction between NO_2 and ammonia.

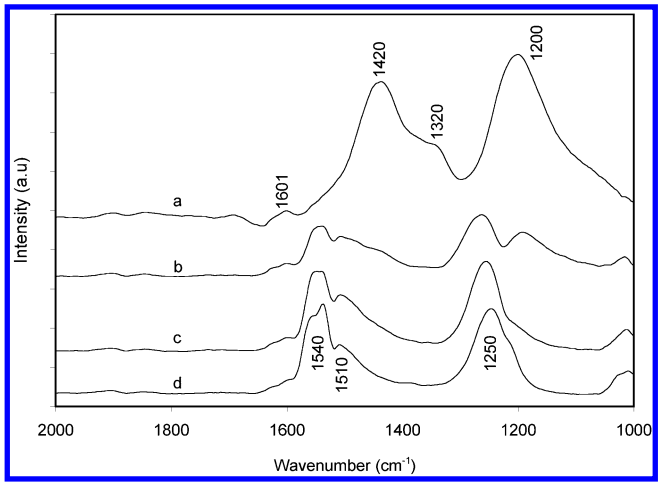

Figure 11. IR spectra of $MnO_x(0.3)-CeO_2(923)$ prepared by the CA method in a flow of 1000 ppm NO + 1000 ppm NH_3 + 2% O_2/He at (a) 298, (b) 393, (c) 423, and (d) 453 K.

IR Spectra of $MnO_x(0.3)-CeO_2(923)$ in a Flow of NO + NH_3 + O_2/He. To identify the species present on the catalyst under reaction conditions, IR spectra were recorded when $MnO_x(0.3)-CeO_2(923)$ was heated from room temperature to 453 K in a flow of NO + NH_3 + O_2/He. As shown in Figure 11, the bands due to nitrite and coordinated NH_3 species were observed at 1601, 1420, 1320, and 1200 cm^{-1} at room temperature. Raising the temperature resulted in a decrease in the band intensities of nitrite and coordinated NH_3 (1200 cm^{-1}), while a peak at 1510 cm^{-1} appeared which was due to amide species (Figure 11b). With an increase in temperature to 423 K, the nitrite and coordinated ammonia species diminished, and the bands at 1540 and 1250 cm^{-1}, which were attributed to the nitrate species, increased with temperature. As noted already, the band at 1510 cm^{-1} in Figure 11c,d was not due to amide, but was probably due to nitrate species formed by NO_x or the oxidation of ammonia at higher temperatures.

4. Discussion

Our previous work[30] has shown that the $MnO_x(0.3)-CeO_2(923)$ catalyst is more active than all known catalysts for low-temperature SCR of NO with NH_3. Nearly 100% NO conversion was obtained under a high space velocity (GHSV = 42 000 h^{-1}). NO conversions on MnO_x-CeO_2 catalysts were much higher than on pure CeO_2 and MnO_x. This indicated that there existed strong interactions between the manganese and cerium oxides which resulted in the high activity. The manganese oxide phase was not detected by XRD for all the catalysts studied. This is further indication of strong interactions. Kapteijn et al.[58] investigated the activity and selectivity of pure manganese oxides for SCR of NO by ammonia and found that the activity and selectivity of N_2 of the unsupported manganese oxide were determined by the oxidation state and the degree of crystallinity, and that Mn_2O_3 exhibited the highest selectivity for nitrogen. It is known that different calcination temperatures result in different oxidation states of manganese, so the calcination temperature affects the activity and selectivity of SCR of NO by NH_3. XPS studies directly showed that different manganese states were detected. From Table 3, it can be seen that the concentration of Mn^{2+} increased with calcination temperature, which is consistent with the result of ESR study. The concentration of Mn^{4+} decreased with calcination temperature, while there was not much change in the concentration of Mn^{3+}. From our previous study, we found that the selectivity for N_2O decreased with calcination temperature; therefore, it can be concluded that the formation of N_2O was related to Mn^{4+}, because the concentration of MnO_2 decreased with calcination temperature. XRD of $MnO_x(0.3)-CeO_2(923)$ prepared by different methods was shown in Figure 3. It is obvious that the XRD intensity of the catalyst prepared by the CA method was the lowest among the three methods used in this work, which was consistent with the mean crystallite sizes of the cubic phase. Consequently, the catalyst prepared by the CA method had the highest activities.[30] On the basis of the activity and characterization results, it can be concluded that at least three kinds of Mn phases existed in the MnO_x-CeO_2 catalysts that were prepared by the CA method: (1) aggregated MnO_x species on the support CeO_2, (2) highly dispersed MnO_x with strong interaction with CeO_2, and (3) Mn atoms incorporated into the CeO_2 lattice. Any oxygen vacancy formed in the CeO_2 lattice due to the incorporation of Mn atoms would adsorb and activate molecular oxygen to form active oxygen species. So, the high activity of the $MnO_x(0.3)-CeO_2(923)$ catalysts is attributed to the highly dispersed Mn species and the more active oxygen species that was formed. Imamura et al.[68] found that the activity of a physical mixture of Mn_2O_3 and CeO_2 in wet air oxidation of ammonia was lower than that of coprecipitated $Mn_2O_3-CeO_2$. This observation suggests that there exists a synergistic mechanism between the manganese and cerium oxides. When CeO_2 and Mn_2O_3 are allowed to contact each other, they interact easily, with isolated Mn^{2+} species appearing even at temperatures as low as 423 K. This means that Mn, although in small amounts, migrates quite easily into the CeO_2 matrix and is reduced.

The FTIR spectra presented already indicated that NO, NO_2, nitrite, and nitrate species were adsorbed on the $MnO_x(0.3)-CeO_2(923)$ catalyst after the sample was treated with NO/He, NO + O_2/He, and NO_2/He. The NO adsorption was very weak. The presence of O_2 increased NO adsorption on the $MnO_x(0.3)-CeO_2(923)$ catalyst. The results indicated that NO could be adsorbed and then oxidized to NO_2, nitrite, and nitrate in the presence of O_2 on $MnO_x(0.3)-CeO_2(923)$. This result is similar to the results obtained on CuO/Al_2O_3, CrO_x/TiO_2, MnO_x/Al_2O_3, and zeolite catalysts[14,15,44,47,71] but different from that obtained on vanadia-based catalyst.[1] Most researchers have reported that no nitrogen oxide adspecies were formed on the vanadia catalyst at 673 K. The addition of cerium oxide significantly enhanced the formation of NH_2 (Figure 7). Because the NO_2 and nitrate species were also observed when NO + O_2 was passed over pure cerium and manganese oxides, the NO_x adspecies on $MnO_x(0.3)-CeO_2(923)$ catalyst may be bound to both manganese and cerium sites.[35] After NH_3/He was passed over the NO_x-adsorbed $MnO_x(0.3)-CeO_2(650)$ catalyst at 393 K, NO_2 and the nitrite species decreased and disappeared, indicating that these NO_x adspecies had been reduced by NH_3.

It was shown that NH_3 adsorbed on both Lewis and Brönsted acid sites on $MnO_x(0.3)-CeO_2(923)$, resulting in coordinated NH_3, NH_4^+ ions, and the formation of NH_2 and other intermediates of ammonia oxidation. The number of coordinated NH_3 species is much higher than NH_4^+ ions. Moreover, an NH_2 species was formed by H-abstraction from coordinated NH_3. The coordinated NH_3 and NH_2 species were present on both Mn^{3+} and Al^{3+} sites.[44] Apparently, H-abstraction was difficult at low temperatures, but the amide species reacted rapidly. On the other hand, at 423 K, the amount of NH_2 increased considerably. The result agreed with results on the NH_3 adsorption and reaction on CuO/Al_2O_3 by Centi et al.,[14] MnO_x/Al_2O_3 by Kijlstra et al.,[44] and CuO/TiO_2 by Ramis et al.[15] These authors also proposed that the SCR reaction proceeds via the amide intermediate. After ammonia was adsorbed on the $MnO_x(0.3)-$

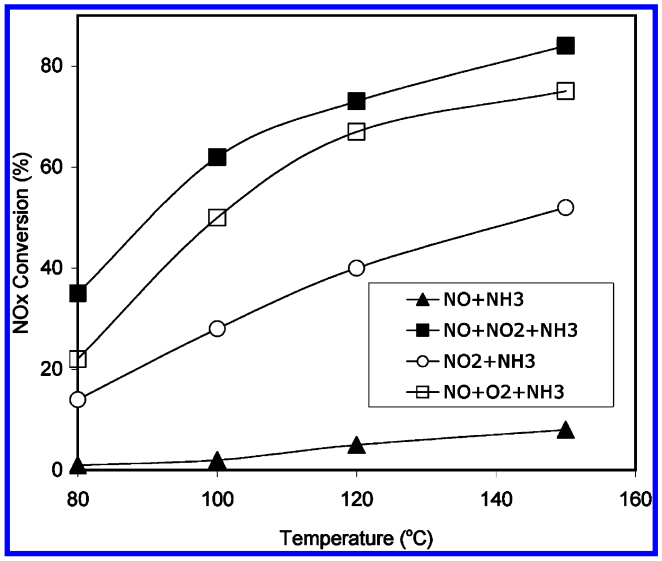

Figure 12. Catalytic activities on $MnO_x(0.3)-CeO_2(923)$ prepared by the CA method for the reactions of NO + NH_3 (1500 ppm NO and 1000 ppm NH_3), NO + NH_3 + O_2 (1000 ppm NO, 1000 ppm NH_3, and 2% O_2), NO_2 + NH_3 (750 ppm NO and 1000 ppm NH_3), NO + NO_2 + NH_3 (500 ppm NO, 500 ppm NO_2, and 1000 ppm NH_3) under the conditions of 0.2 g of sample and 500 mL/min total flow rate.

$CeO_2(923)$ catalyst, coordinated NH_3, nitrite, and NH_4^+ were formed, but the amount of the NH_4^+ ions was very small. So, the reaction between NO_x and coordinated NH_3 and amide species predominates. After NO + O_2 was passed over the catalysts, the coordinated ammonia and amide that were adsorbed on the catalyst quickly vanished. To study the reactivity between NH_3 and NO, NO + O_2, and NO + NO_2, the reactions NO + O_2 + NH_3, NO_2 + NO + NH_3, and NH_3 + NO were investigated (Figure 12). The activity results show that the reaction rates of NO + O_2 + NH_3 and NO_2 + NO + NH_3 were much higher than those of NO + NH_3 and NO_2 + NH_3, but the reaction of NO_2 + NO + NH_3 has the highest activity, which is consistent with the report of Koebel et al.[60]

From the IR study of our previous work,[35] NO_x could be adsorbed strongly on MnO_x and CeO_2, but there were some differences. First, the species adsorbed on MnO_x were mainly nitrate, while for CeO_2, abundant nitrite species could be formed. Meanwhile, the transformation rate of NO^- into nitrate and nitrite is different for the two catalysts. The rate for MnO_x is much faster than that for CeO_2, so the main function of MnO_x was to oxidize NO to nitrate or nitrite, while CeO_2 mainly produced nitrite species. On the basis of this analysis, it can be understood that the combination of manganese and cerium can significantly enhance the SCR activity. Machida[48] studied the NO_x adsorption over MnO_x-CeO_2 mixed oxides and proposed that the role of manganese ions substituted in the CeO_2 lattice was to act as a catalyst for NO oxidation in the presence of O_2. On the other hand, Ce ions provide a number of adsorption sites on the surface, because the moderate basicity allows surrounding oxide ions to react readily with NO_x, which is then oxidized.

The mechanism of surface reaction of NO_x on mixed-oxide catalysts has been studied extensively in the past.[1] Different hypotheses have been proposed for the mechanism,[1,24,49−52,66,67] including the reaction between the ammonium ion and adsorbed NO_2, the reaction between an amide and gaseous NO, and the reaction between coordinated ammonia and a species generated by the spillover of NO on the support. The formation of NH_2 has been suggested by Ramis et al. as the key step in the mechanism of NO reduction on $V-TiO_2$.[53] Gaseous NO reacts with NH_2 to form a nitrosamine (NH_2NO) that decomposes into N_2 + H_2O. Galardoni et al.[54,55] proposed in a theoretical study that the adsorbed NH_4^+ species reacts with NO on the surface of vanadium oxide to produce NH_2NO, which may then isomerize to yield N_2 and H_2O. Kobayashi et al.[56] proposed several species derived from NH_2NO as reaction intermediates in a theoretical study of the gas-phase reaction of NH_3 and NH_4^+ with NO. Anstrom et al.[57] reported a mechanism by using density functional theory calculations that nitric oxide reacted with adsorbed NH_4^+ to yield NH_3HNO, which then reacted further to yield the NH_2NO. The NH_2NO decomposed to give N_2 and H_2O. Kapteijn et al.[58] indicated that the interaction of NO, NH_3, and O_2 over manganese oxide could be explained by a model where the NH_3 was successively dehydrogenated by surface oxygen. In this model, the intermediate ($-NH_2$) could react with NO to form N_2, while $-NH$ or $-N$ species could only react with NO to give N_2O. Kijlstra et al.[12] studied the mechanism of SCR of NO with ammonia at low temperatures on MnO_x/Al_2O_3 catalyst. They proposed that the reaction starts with the adsorption of NH_3 on a Lewis acid and subsequently transforms into NH_2; the NH_2 would then react with gas-phase NO (an ER mechanism) and nitrite intermediates on the surface (a LH mechanism). Sachtler et al.[59] proposed a different mechanism on Fe-ZSM-5 catalysts. They assumed that NO and NO_2 reacted with H_2O and NH_3 to form ammonium nitrite which decomposed to N_2. Koebel et al.[60,61] investigated the low-temperature behavior of the NH_3 SCR process on V_2O_5/TiO_2 catalyst with feed gases containing both NO and NO_2. The mixed oxides of nitrogen (NO + NO_2) in the feed mixture increased the reaction rate significantly, which is consistent with our results (Figure 12). The authors[60] disregarded the idea that N_2O_3 directly reacted with NH_3 because the thermodynamic stability of N_2O_3 would give little support to reaction 5.

$$NO + NO_2 \rightarrow N_2O_3 \quad (5)$$

Finally, Koebel et al.[60,61] proposed a mechanism similar to that of Ramis et al.,[53] except in the step of reoxidation of V^{4+} to V^{5+}. In Koebel et al., the reoxidation of the catalyst was done by NO_2, and then NO_2 converted to HNO_2, while in Ramis et al., the reoxidation of the catalyst was done by O_2. Thus, in Koebel et al.,[60,61] the SCR is performed with NO_2 yielding nitrous acid HNO_2. The nitrous acid (HNO_2) then reacts with ammonia; a similar process was also proposed by Sachtler et al.[59]

On the basis of the present investigation as well as the earlier reports,[49−52,53,59−61] the SCR reaction of NO with NH_3 on the $MnO_x(0.3)-CeO_2(923)$ catalyst most probably takes place according to the so-called amide−nitrosamide mechanism. The following is the most likely mechanism on the basis of our FTIR studies (note the (a) refers to adsorbate):

$$^1/2O_2(g) \rightarrow O(a) \quad (6)$$

$$2NH_3(g) \rightarrow 2NH_3(a) \quad (7)$$

$$NH_3(a) + O(a) \rightarrow NH_2(a) + OH(a) \quad (8)$$

$$NO(g) + O(a) \rightarrow NO_2(a) \quad (9)$$

$$NH_2(a) + NO(g) \rightarrow NH_2NO(a) \rightarrow N_2(g) + H_2O(g) \quad (10)$$

$$NH_3(a) + NO_2(a) \rightarrow N_2 + H_2O + OH(a) \quad (11)$$

$$2OH(a) \rightarrow H_2O + O(a) \quad (12)$$

In the SCR reaction, gaseous NH_3 molecules are first adsorbed on the $MnO_x(0.3)-CeO_2(923)$ catalyst to form coordinated NH_3 and NH_2. NO molecules are also adsorbed on the $MnO_x(0.3)-$

CeO_2(923) catalyst and then oxidized to nitrate and nitrite. The reaction of NH_2 and NO and then the formation of nitrosamine (NH_2NO) is a typical SCR mechanism reported for V_2O_5/TiO_2- and manganese-based catalysts. The NH_2NO decomposes to give N_2 and H_2O. At high temperatures, N_2O was produced by the reaction of NH_3 with nitrate. In addition to the mechanism mentioned already, the reaction between NO_2 and NH_3 species also occurred under the reaction conditions (Figure 10). In our entire FTIR experiment, although NH_4^+ cannot be detected, the existence of the intermediate NH_4NO_2 is also a possibility because of the fast transformation of the intermediate. The nitrous acid was produced by a reoxidation reaction or disproportionation of $2NO_2$ with H_2O.[60] The nitrous acid reacts with ammonia and then produces ammonium nitrite, which is equivalent to the hydrate of nitrosamine NH_2NO.[60] Both ammonium nitrite and nitrosamine are unstable and probable intermediates in many proposed NH_3 SCR mechanisms.

5. Conclusions

Ammonia molecules were adsorbed on the $MnO_x(0.3)-CeO_2$(923) catalyst to form NH_4^+ and coordinated NH_3. At the same time, NH_2 was observed because of H-abstraction. Three kinds of Mn phases existed in the MnO_x-CeO_2 catalyst prepared by the CA method: (1) aggregated Mn_2O_3 on the CeO_2 support, (2) highly dispersed Mn_2O_3 with strong interactions with CeO_2, and (3) Mn atoms incorporated into the CeO_2 lattice. Any oxygen vacancy formed in the CeO_2 lattice by the incorporation of Mn atoms would adsorb and activate the molecular oxygen to form active oxygen species. So, the high activity for the $MnO_x(0.3)-CeO_2$(923) catalysts is attributed to the highly dispersed Mn species and the more-active oxygen species that is formed. A mechanistic pathway for this reaction was proposed on the basis of earlier findings and the FTIR results obtained in this work. The initial step was the adsorption of NH_3 on the Lewis acid sites of the catalyst, followed by reaction with nitrite species to produce N_2 and H_2O. Possible intermediates are proposed, and all the intermediates could transform into NH_2NO, which could further react to produce N_2 and H_2O.

Acknowledgment. This work was supported by NSF and EPRI.

References and Notes

(1) Bosch, H.; Janssen, F. *Catal. Today* **1988**, *2*, 369.
(2) Bauerle, G. L.; Wu, S. C.; Nobe, K. *Ind. Eng. Chem. Prod. Res. Dev*. **1978**, *17*, 123.
(3) Wong, W. C.; Nobe, K. *Ind. Eng. Chem. Prod. Res. Dev*. **1986**, *25*, 179.
(4) Janssen, F.; Kerkhof, F.; Bosh, H.; Ross, J. R. H. *J. Phys. Chem*. **1987**, *91*, 5921.
(5) Byrne, J. W.; Chen, J. M.; Speronello, B. K. *Catal. Today* **1992,** *13*, 33.
(6) Ramis, G.; Busca, G.; Bregani, F. *Catal. Lett*. **1993**, *139*, 353.
(7) Chen J. P.; Yang R. T. *Appl. Catal*. **1992**, *80*, 135.
(8) Busca, G.; Lietti, L.; Ramis, G.; Berti, F. *Appl. Catal., B* **1988**, *18*, 1.
(9) Bauerle, G. L.; Wu, S. C.; Nobe, K. *Ind. Eng. Chem. Prod. Res. Dev*. **1975**, *14*, 268.
(10) Singoredjo, L.; Korver, R.; Kapteijn, F.; Moulijn, J. A. *Appl. Catal., B* **1992**, *1*, 297.
(11) Jang, B. W. L.; Spivey, J. J.; Kung, M. C.; Kung, H. H. *Energy Fuels* **1997**, *11*, 299.
(12) Kijlstra, W. S.; Brands, D. S.; Smit, H. I.; Poels, E. K.; Bliek, A. *J. Catal.* **1997**, *171*, 219.
(13) Kijlstra, W. S.; Poels, E. K.; Bliek, A.; Weckhuysen, B. M.; Schoonheydt, R. A. *J. Phys. Chem. B* **1997**, *101*, 309.
(14) Centi, G.; Perathoner, S.; Biglino, D.; Giamello, E. *J. Catal*. **1995**, *151*, 75.
(15) Ramis, G.; Yi, L.; Busca, G.; Turco, M.; Kotur, E.; Willey, R. J. *J. Catal*. **1995**, *157*, 523.
(16) Kato, A.; Matsuda, S.; Nakajima, F.; Imanri, M.; Watanabe, Y. *J. Phys. Chem*. **1981**, *85*, 1710.
(17) Kasaoka, S.; Sasaoka, E.; Iwasaki, H. *Bull. Chem. Soc. Jpn*. **1989**, *62*, 1226.
(18) Pasel, J.; Kässner, P.; Montanari, B.; Gazzano, M.; Vaccari, A.; Makowski, W.; Lojewski, T.; Dziembaj, R.; Papp, H. *Appl. Catal., B* **1998**, *18*, 199.
(19) Ozkan, U. S.; Cai, Y.; Kumthekar, M. W. *J. Catal*. **1994**, *149*, 390.
(20) Chen, J. P.; Yang, R. T.; Buzanowski, M. A.; Cichanowicz, J. E. *Ind. Eng. Chem. Res*. **1990**, *29*, 1431.
(21) Singoredjo, L.; Korver, R.; Kapteijn, F.; Moulijn, J. A. *Appl. Catal., B* **1992**, *1*, 297.
(22) Zhu, Z.; Liu, Z.; Niu, H.; Liu, S. *J. Catal*. **1999**, *187*, 245.
(23) Fabrizioli, P.; Burgi, T.; Baiker, A. *J. Catal*. **2002**, *206*, 143.
(24) Richter, M.; Trunschke, A.; Bentrup, U.; Brzezinka, K.-W.; Schreier, E.; Schneider, M.; Pohl, M.-M.; Fricke, R. *J. Catal*. **2002**, *206*, 98.
(25) Notoya, F.; Su, C.; Sasako, E.; Nojima, S. *Ind. Eng. Chem. Res*. **2000**, *40*, 3732.
(26) Long, R. Q.; Yang, R. T.; Chang, R. *Chem. Commun*. **2002**, *5*, 452.
(27) Taylor, K. C. *Catal. Rev.—Sci. Eng*. **1993**, *35*, 47.
(28) Logan, A. D.; Shelef, M. *J. Mater. Res*. **1994**, *9*, 468.
(29) Liu, W.; Sarofim, A. F.; Flytzani-Stephanopoulos, M. *J. Catal*. **1995**, *53*, 304.
(30) Qi, G.; Yang, R. T. *J. Catal*. **2003**, *217*, 434.
(31) Qi, G.; Yang, R. T. *Chem. Commun*. **2003**, *7*, 848.
(32) Klug, H. P.; Alexander, L. E. *X-ray Diffraction Procedures*; Wiley: New York, 1954.
(33) Shan, W.; Luo, M.; Ying, P.; Shen, W.; Li, C. *Appl. Catal., B* **2003**, *246*, 1.
(34) Machida, M.; Uto, M.; Kurogi, D.; Kijima, T. *Chem. Mater*. **2000**, *12*, 3158.
(35) Qi, G.; Yang, R. T.; Chang, R. *Appl. Catal., B* **2004**, *51*, 93.
(36) EPRI and Oglethorpe Power Corporation. *Advanced NO_x Catalysts Development Update*; Report No. 1004889; Palo Alto, CA, and Juliette, GA, 2003.
(37) Xu, J.; Luan, Z.; Wasowicz, T.; Kevan, L. *Microporous Mesoporous Mater*. **1998**, *22*, 179.
(38) Kijlstra, W. S.; Poels, E. K.; Bliek, A.; Weckhuysen, B. M.; Schoonheydt, R. A. *J. Phys. Chem. B* **1997**, *101*, 309.
(39) El Mkami, H.; Deroide, B.; Zanchetta, J. V.; Rumori, P.; Abidi, N. *J. Non-Cryst. Solids* **1996**, *208*, 21.
(40) Velu, S.; Shah, N.; Jyothi, T. M.; Sivasanker, S. *Microporous Mesoporous Mater.* **1999**, *33*, 61.
(41) Ramis, G.; Busca, G.; Lorenzelli, V.; Forzatti, P. *Appl. Catal*. **1990**, *64*, 243.
(42) Laane, J.; Ohlsen, J. R. *Prog. Inorg. Chem*. **1980**, *27*, 465.
(43) Aylor, A. W.; Lobree, L. J.; Reimer, J. A.; Bell, A. T. *J. Catal*. **1997**, *170*, 390.
(44) Kijlstra, W. S.; Brands, D. S.; Smit, H. I.; Poels, E. K.; Bliek, A. *J. Catal*. **1997**, *171*, 208.
(45) Chen, H.-Y.; Voskoboiniko, T.; Sachtler, W. M. H. *J. Catal*. **1998**, *180*, 171.
(46) Curry-Hyde, H. E.; Mush, H.; Baiker, A.; Schraml-Marth, M.; Wokaun, A. *J. Catal*. **1992**, *133*, 397.
(47) Long, R. Q.; Yang, R. T. *J. Catal*. **2000**, *190*, 22.
(48) Machida, M. *Catal. Surv. Jpn*. **2002**, *5*, 91.
(49) Komatsu, T.; Ogawa, T.; Yashima, T. *J. Phys. Chem*. **1995**, *99*, 13053.
(50) Salker, A. V.; Weisweiler, W. *Appl. Catal., A* **2000**, *203*, 221.
(51) Centi, G.; Perathoner, S. *J. Catal*. **1995**, *152*, 93.
(52) Park, T. S.; Jeong, S. K.; Hong, S. H.; Hong, S. C. *Ind. Eng. Chem. Res*. **2001**, *40*, 4491.
(53) Ramis, G.; Busca, G.; Bregani, F.; Forzatti, P. *Appl. Catal*. **1990**, *64*, 259.
(54) Gilardoni, F.; Weber, J.; Baiker, A. *Int. J. Quantum Chem*. **1997**, *61*, 683.
(55) Gilardoni, F.; Weber, J.; Baiker, A. *J. Phys. Chem. A* **1997**, *101*, 6069.
(56) Kobayashi, Y.; Tajima, N.; Hirao, K. *J. Phys. Chem. A* **2000**, *104*, 6855.
(57) Anstrom, M.; Topsøe, N.-Y.; Dumesic, J. A. *J. Catal*. **2003**, *213*, 115.
(58) Kapteijn, F.; Singoredjo, L.; Andreini, A.; Moulijn, J. A. *Appl. Catal., B* **1994**, *3*, 173.
(59) Sun, Q.; Gao, Z.-X.; Chen, H.-Y.; Sachtler, W. M. H. *J. Catal*. **2001**, *201*, 89.
(60) Koebel, M.; Elsener, M.; Madia, G. *Ind. Eng. Chem. Res*. **2001**, *40*, 52.
(61) Koebel, M.; Madia, G.; Raimondi, F.; Wokaun, A. *J. Catal*. **2002**, *209*, 159.

(62) *Handbook of X-ray Photoelectron Spectroscopy*; Wagner, C. D., Riggs, W. M., Davis, L. E., Moulder, J. F., Mullerberg, G. E., Eds.; Perkin-Elmer Corp.: Eden Prairie, MN, 1979.
(63) Nesbitt, H. W.; Banerjee, D. *Am. Mineral.* **1998**, *83*, 305.
(64) Fabrizioli, P.; BuÜrgi, T.; Baiker, A. *J. Catal*. **2002**, *207*, 88.
(65) Kapteijn, F.; van Langeveld, A. D.; Moulijn, J. A.; Andreini, A.; Vuurman, M. A.; Turek, A. M.; Jehng, J. M.; Wachs, I. E. *J. Catal*. **1994**, *150*, 94.
(66) Kijlstra, W. S.; Brands, D. S.; Poels, E. K.; Bliek, A. *Catal. Today* **1999**, *50*, 133.
(67) Marbán, G.; Fuertes, A. B. *Catal. Lett*. **2002**, *84*, 13.
(68) Imamura, S.; Doi, A.; Ishida, S. *Ind. Eng. Chem. Prod. Res. Dev*. **1985**, *24*, 75.
(69) Smirniotis, P. G.; Peña, D. A.; Uphade, B. S. *Angew. Chem., Int. Ed*. **2001**, *40*, 2479.
(70) Peña, D. A.; Uphade, B. S.; Smirniotis, P. G. *J. Catal*. **2004**, *221*, 421.
(71) Trovarelli, A. *Catal. Rev.—Sci. Eng*. **1996**, *38*, 439.
(72) Ramis, G.; Larrubia, M. A. *J. Mol. Catal. A: Chem.* **2004**, *215*, 161.
(73) Larrubia, M. A.; Ramis, G.; Busca, G. *Appl. Catal*., *B* **2001**, *30*, 101.
(74) Larrubia, M. A.; Ramis, G.; Busca, G. *Appl. Catal*., *B* **2000**, 27, L145.
(75) Matralis, H. K.; Ciardelli, M.; Ruwet, M.; Grange, P. *J. Catal*. **1995**, *157*, 368.